

# All-Analog Adaptive Equalizer for Coherent Data Center Interconnects

Nandakumar Nambath, Rakesh Ashok, Sarath Manikandan, Nandish Bharat Thaker, Mehul Anghan, Rashmi Kamran, Saurabh Anmadwar, and Shalabh Gupta

**Abstract**—We present the detailed architecture of an all-analog adaptive equalizer for low-power analog signal processing based coherent optical dual-polarization quadrature phase-shift keying transceivers. The proof of concept equalizer uses the constant modulus algorithm for weight coefficient update. The equalizer, implemented in a 130 nm SiGe BiCMOS technology for 100 Gb/s operation, occupies  $\sim 1.4 \text{ mm} \times 1.35 \text{ mm}$  area and draws 1 A current from a 2.5 V supply. Its functionality is validated experimentally for data rates up to 40 Gb/s and by using post-layout circuit simulations for data rates up to 100 Gb/s. The equalizer output after processing with a behavioral Costas loop-based carrier phase recovery and compensation module shows bit error rates well within the hard-decision forward error correction limit for 40 Gb/s single-mode fiber links of length up to 10 km. Performance and power consumption of the equalizer are expected to improve when implemented in advanced CMOS or FinFET technologies. The simple architecture of the analog domain equalizer makes it suitable for analog coherent short-reach interconnects with length less than 10 km and carrier wavelengths of either 1310 nm or 1550 nm.

**Index Terms**—Analog coherent receiver, adaptive equalizer, fractionally spaced equalizer, analog signal processing, constant modulus algorithm, BiCMOS integrated circuits.

## I. INTRODUCTION

**D**ATA center interconnects (DCIs) are expected to carry around 80% of the global Internet traffic, which is estimated to increase two-fold from today's traffic of 200 EB/month, by 2022 [1, 2]. To support the increased traffic, DCI interface speeds are projected to cross 1.6 Tb/s in the near future [3]. To meet the current needs, 4-level pulse amplitude modulation (PAM-4) format based intensity modulation-direct detection (IMDD) transceivers with electronics operating at 56 GBd rate are being standardized [3, 4]. However, IMDD techniques are anticipated to give way to the transmission of more spectrally efficient modulation formats through single-mode fiber (SMF) in short-reach links [5, 6], mainly due to

data rate scalability limitations [7]. As opposed to IMDD, coherent techniques aid in achieving data rate scalability together with a better receiver sensitivity [8]. Coherent links that use higher order modulation formats and polarization multiplexing help to achieve higher capacities and longer channel lengths, relying heavily on digital signal processing (DSP) to overcome the impairments added by the fiber channel. However, such links require high-speed, high-precision analog-to-digital converters (ADCs) to digitize the received signals after optical-to-electrical (O/E) conversion followed by high-speed DSP. Therefore, usage of the ADC+DSP approach becomes prohibitive for DCIs due to a huge amount of power consumption and complexity involved in this solution [9].

To overcome this issue an analog domain processing based solution was proposed, for the first time, in our previous work [10]. Since then a few other solutions using the analog domain (or DSP-free) processing for coherent optical links have been reported [9, 11–15]. For instance, [11] discusses an analytical study on the feasibility of DSP-free homodyne dual-polarization quadrature phase-shift keying (DP-QPSK) receivers for DCIs. The reported polarization multiplexing based architecture uses a simplified  $2 \times 2$  equalizer, for correcting small amounts of dispersion and bandwidth limitations, the weight coefficients of which can be updated by using either the constant modulus algorithm (CMA) or a least mean square algorithm. In another study, the validation results of a proof-of-concept DSP-free coherent transceiver for DCIs that uses dual polarization-16 quadrature amplitude modulation format has been reported [12]. More recently, an analog coherent engine, working up to 400 Gb/s dissipating 2 W of power, that uses analog signal processing followed by a feed-forward equalizer filter for improving signal quality for 15 m SMF has been demonstrated [9].

Studies on low-power analog coherent optics, based on optical phase-locked loop (OPLL), which work for very short distances due to the choice of low dispersion, but high attenuation O-band have also been reported [6, 13]. Another work demonstrates a 40 Gb/s OPLL based analog coherent binary phase-shift keying receiver that uses the integration of electronic and photonic integrated circuits (ICs) to eliminate the usage of DSP for carrier offset removal [14]. Further, a technique to achieve carrier phase synchronization using analog signal processing based IC, phase modulator, and tunable lasers has been demonstrated [16]. These receivers (in [14, 16]) use OPLL for phase and frequency offsets correction to achieve significant power savings by removing DSP completely.

N. Nambath is with the School of Electrical Sciences, Indian Institute of Technology Goa, Ponda – 403401, India (e-mail: npnandakumar@iitgoa.ac.in).

R. Ashok, S. Manikandan, R. Kamran, and S. Gupta are with the Department of Electrical Engineering, Indian Institute of Technology Bombay, Mumbai – 400076, India (email: rakesh.ashok@iitb.ac.in; sarath.m@iitb.ac.in; rashmikamran@ee.iitb.ac.in; shalabh@ee.iitb.ac.in).

N. B. Thaker and S. Anmadwar are with Intel Technology India Pvt. Ltd., Bengaluru – 560103, India (e-mail: nandish.bharat.thaker@intel.com; saurabh.r.anmadwar@intel.com).

M. Anghan is with Rambus Chip Technologies India Pvt. Ltd., Bengaluru – 560029, India (e-mail: manghan@rambus.com).

N. B. Thaker, M. Anghan, and S. Anmadwar were with the Department of Electrical Engineering, Indian Institute of Technology Bombay, Mumbai – 400076, India when this work was carried out.

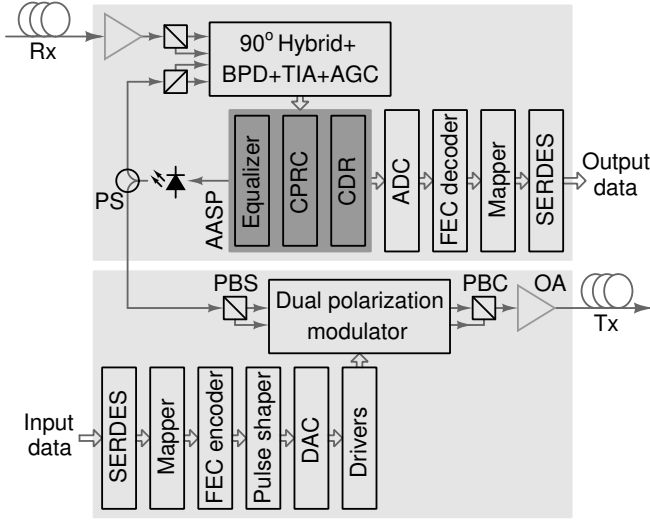


Fig. 1. Block diagram of the proposed transceiver for coherent optical links with a dual polarization, phase modulated carrier. BPD: balanced photo-diodes, TIA: trans-impedance amplifier, AGC: automatic gain control, PS: power splitter, AASP: all-analog signal processing, CPRC: carrier phase recovery and compensation, CDR: clock and data recovery, ADC: analog-to-digital converter, FEC: forward error correction, SERDES: serializer/deserializer, PBS: polarization beam splitter, PBC: polarization beam combiner, OA: optical amplifier, and DAC: digital-to-analog converter.

From the literature, it may be summarized that miniaturized analog coherent transceiver using electronic and photonic integration is a solution for the power dissipation-size-cost problem in the future generation DCIs. The block diagram of such a transceiver is given in Fig. 1. In a coherent optical transceiver, a major portion of the power is consumed by the receiver electronics which can be reduced significantly if the main signal processing operations—equalization, carrier phase recovery and compensation (CPRC), and clock and data recovery (CDR) are done in the analog domain as shown in the figure. It may be observed that the ADC comes after the three main operations in the receiver data path, relaxing the speed and precision constraints on it, which helps in reducing the overall complexity and power consumption of the transceiver. In the receiver side, an equalizer is used to mitigate the effects of polarization mode dispersion (PMD) and chromatic dispersion (CD). A CPRC is required to compensate for the phase and frequency mismatches between the transmitter and receiver lasers, and a CDR is required for clock recovery from the received signals.

Equalizer being the major power dissipating block in a coherent optical receiver [17], we studied analog domain implementation of the equalizer as a proof-of-concept validation of the analog processing based transceiver. It may also be seen from the literature that analog domain processing is an attractive choice for low-power equalization in various types of high-speed links [18–27]. Specifically for optical links, a CMOS receiver with a continuous-time linear equalizer for 30 Gb/s links is reported in [26] and a monolithic optoelectronic IC designed in a 130 nm CMOS process that uses analog domain slope detection based adaptive equalizer is demonstrated in [27] for links with a carrier of 850 nm wavelength.

However, the first all-analog adaptive equalizer for DP-QPSK coherent optical system that uses a CMA algorithm for weight coefficient update was demonstrated in our previous work [28]. In this paper, we report the proof-of-concept demonstration of the equalizer operating at a rate as high as 40 Gb/s. We also present the detailed architecture of the equalizer and mention the practical constraints, as well as future directions, associated with the all-analog signal processing approach.

The remainder of this paper is organized as follows. Section II gives the detailed architecture of the CMA Equalizer. Section III describes the block-wise implementation and integration of a two-tap equalizer using 130 nm BiCMOS technology. Section IV discusses the details of the experimental validation of the equalizer at 40 Gb/s and post-layout circuit simulation results of the equalizer at 100 Gb/s. Section V draws the conclusions of the paper.

## II. SYSTEM OVERVIEW

The O/E front-end of a DP-QPSK receiver will give out four electrical signals corresponding to the in-phase and quadrature-phase components of the X and Y polarizations. These four signals will not be independent of each other due to CD, PMD, polarization rotation, and polarization-dependent loss. Hence, a multi-dimensional equalizer that has four inputs and four outputs need to be used to process all the signals jointly. The equalizer should adaptively mitigate the dispersion effects of the fiber, which is a time-varying phenomenon. To adapt the equalizer weight coefficients, the CMA algorithm [29] is used, which is one of the simplest blind equalization algorithms that can be used with DP-QPSK signals.

Fig. 2(a) shows the architecture of the equalizer that uses the CMA algorithm to adapt the weight coefficients. The equalizer has a feed-forward block and an error generator. It has inputs  $x$  and  $y$  and outputs  $x_{eq}$  and  $y_{eq}$  which are complex signals corresponding to the X and Y polarizations, respectively. The feed-forward block has four transversal filters with coefficients  $h_{xx}$ ,  $h_{xy}$ ,  $h_{yx}$ , and  $h_{yy}$  which are arranged as a butterfly structure. This structure generates equalized output signals,  $x_{eq}$  and  $y_{eq}$  from the inputs, and the CMA error signals  $\varepsilon_x$  and  $\varepsilon_y$ , which are calculated in the error generator. The outputs of the equalizer are given by [30]

$$x_{eq} = \mathbf{h}_{xx}^T \mathbf{x} + \mathbf{h}_{xy}^T \mathbf{y}, \quad (1)$$

$$y_{eq} = \mathbf{h}_{yx}^T \mathbf{x} + \mathbf{h}_{yy}^T \mathbf{y}, \quad (2)$$

where  $\mathbf{x}$  and  $\mathbf{y}$  are vectors containing delayed input signals. The continuous-time update equations of the equalizer weight coefficients are given by [30]

$$h_{xx,k}(t) = \beta \int_0^t x_{eq}(\tau) [1 - |x_{eq}(\tau)|^2] x(\tau - k\tau_d) d\tau, \quad (3)$$

$$h_{xy,k}(t) = \beta \int_0^t y_{eq}(\tau) [1 - |y_{eq}(\tau)|^2] x(\tau - k\tau_d) d\tau, \quad (4)$$

$$h_{yx,k}(t) = \beta \int_0^t x_{eq}(\tau) [1 - |x_{eq}(\tau)|^2] y(\tau - k\tau_d) d\tau, \quad (5)$$

$$h_{yy,k}(t) = \beta \int_0^t y_{eq}(\tau) [1 - |y_{eq}(\tau)|^2] y(\tau - k\tau_d) d\tau, \quad (6)$$

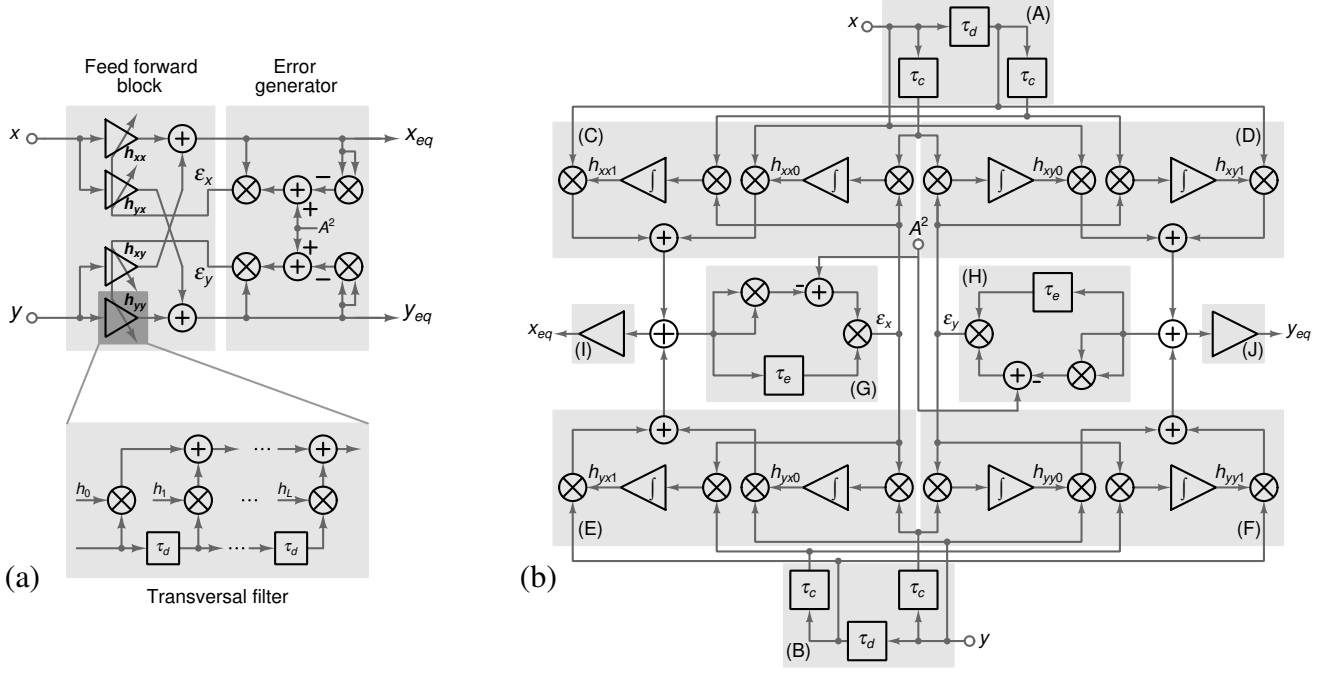


Fig. 2. The constant modulus algorithm based equalizer. (a) The architecture of a multidimensional adaptive equalizer that uses the CMA algorithm. The detailed structure of a transversal filter is shown on the bottom side. (b) Detailed block diagram of a two-tap CMA Equalizer. Blocks: (A) X delay line, (B) Y delay line, (C) X input to X output forward path, (D) X input to Y output forward path, (E) Y input to X output forward path, (F) Y input to Y output forward path, (G) X error generator, (H) Y error generator, (I) X output buffer, and (J) Y output buffer.  $\tau_d$  is the tap delay,  $\tau_c$  is the delay inserted to compensate for the delay mismatch in the forward paths, and  $\tau_e$  is the delay inserted to compensate for the delay mismatch in the error generators.

where  $x = x_I + jx_Q$  and  $y = y_I + jy_Q$  are the X and Y polarization input signals of the equalizer,  $x_{eq} = x_{eq,I} + jx_{eq,Q}$  and  $y_{eq} = y_{eq,I} + jy_{eq,Q}$  are the equalizer outputs in the corresponding polarizations,  $\tau_d$  is the tap delay, and  $0 \leq k \leq L$ , where  $L$  is the total number of delay cells in each transversal filter. The subscripts I and Q represent the in-phase and quadrature-phase components of the signals, respectively.

### III. IMPLEMENTATION DETAILS

A fractionally spaced two-tap continuous-time CMA equalizer for 100 Gb/s DP-QPSK links is designed and fabricated using 130 nm SiGe BiCMOS technology from ST Microelectronics as a proof-of-concept. Fig. 2(b) shows a detailed block diagram of the prototype equalizer, which consists of linear transversal filters, error generators, and weight-update modules. The figure is a block-level translation of the system described by (1)-(6) with a few minor modifications to take care of the circuit level issues discussed in the following sub-section.

#### A. Issues of Delay Mismatch and Signal Swing

Path delay is an inherent problem associated with any circuit which gets worse as the number of circuit blocks in the path is increased. This problem becomes crucial if the circuit has multiple parallel paths. Signal delays through the parallel paths are to be made equal over the desired frequency range. It is evident from (3)-(6) that there are parallel paths in the CMA equalizer. Signals through the parallel paths get multiplied down the signal path. In such cases, delay cells are inserted

in the paths that have lower group delays. In Fig. 2(b) delay cells  $\tau_c$  are inserted to compensate for the delay mismatch in the forward paths and  $\tau_e$  are inserted to compensate for the delay mismatch in the error generators. Equations (3)-(6) assume a normalized single ended signal magnitude which is taken as 100 mV in the circuit. Gains of all the building blocks are scaled according to this signal level. In Fig. 2(b) the expected amplitude is represented by  $A$ , which is 100 mV for a single-ended signal. Taking these into consideration, (3) can be modified as

$$h_{xx,k}(t) = \beta \int_0^t [x_{eq}(\tau) - \tau_e] [A^2 - |x_{eq}(\tau)|^2] x(\tau - k\tau_d - \tau_c) d\tau. \quad (7)$$

Equations (4)-(6) can also be modified in a similar way. It can be concluded from Fig. 2(b) that the main operations in the equalizer are delay, multiplication, addition, and integration. The following sub-section briefly describes design details of basic building blocks of the equalizer.

#### B. Basic Building Blocks of the Equalizer

1) *Delay Cell*: An active delay cell is chosen over a passive delay cell to save chip area and hence, for the ease of routing. The delay cell is implemented by cascading several common emitter (CE) stages followed by a common collector (CC) buffer to drive a large capacitive load. A circuit schematic of the delay cell is shown in Fig. 3. The group delay of the cell  $\tau_d$  with five cascaded CE stages is shown in Fig. 4<sup>1</sup>. The

<sup>1</sup>Unless specified otherwise, all responses of the building blocks are results of post-layout Monte Carlo simulations with 200 runs at 27°C with 50 fF parasitic capacitance at each output node.

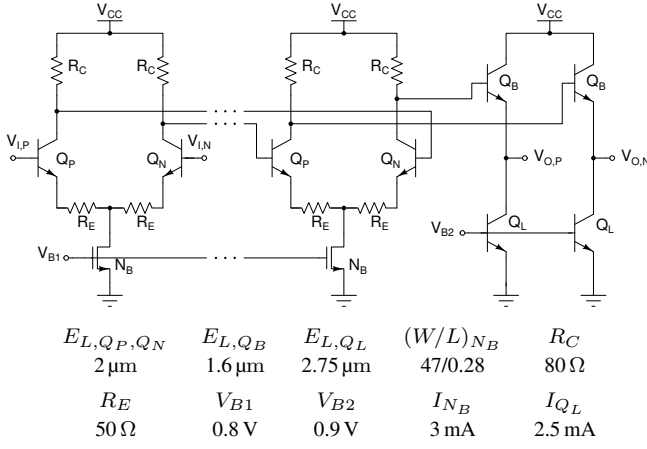


Fig. 3. Schematic of a delay cell. A delay cell with five CE stages followed by a CC buffer has an area of  $\sim 95 \mu\text{m} \times 50 \mu\text{m}$  and a bandwidth of 20.7 GHz.

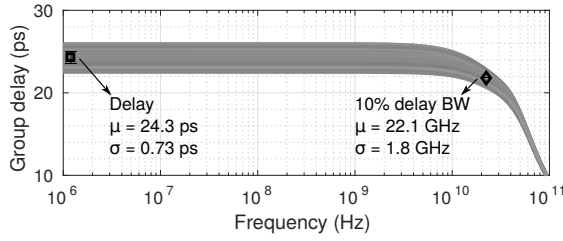


Fig. 4. Group delay response of the delay cell  $\tau_d$ . This cell provides a delay of 24.3 ps and has a 10% delay bandwidth of 22.1 GHz.

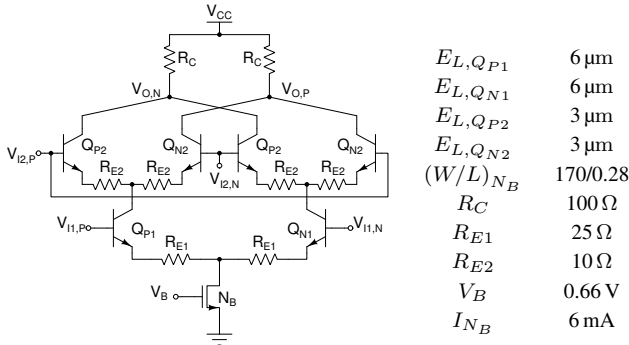


Fig. 5. Schematic of the Gilbert cell multiplier with degeneration resistors. The multiplier occupies an area of  $\sim 40 \mu\text{m} \times 45 \mu\text{m}$ .

delay cell, with an area of  $\sim 95 \mu\text{m} \times 50 \mu\text{m}$ , has a DC gain of  $-1.4 \text{ dB}$ , and a bandwidth of 20.7 GHz. This provides a group delay of 24.3 ps with a 10% delay-bandwidth of 22.1 GHz. The delay cells  $\tau_c$  and  $\tau_e$  are implemented similarly by varying the number of CE stages as per the delay needed.

2) *Multiplier*: The multiplication operation is realized using the Gilbert cell topology [31]. Fig. 5 shows a circuit schematic of the multiplier. The circuit has degeneration resistances to improve the linearity. The multiplier has a DC gain of 7.4 dB and a bandwidth of 20.2 GHz from I1 when I2 is 200 mV, and a DC gain of 6.02 dB and a bandwidth of 17.9 GHz from I2 when I1 is 200 mV. Due to the lower bandwidth of I2 low-speed signals such as filter weight coefficients are applied at this input. DC transfer characteristics of the multiplier shown in Fig. 6. It can be observed that the

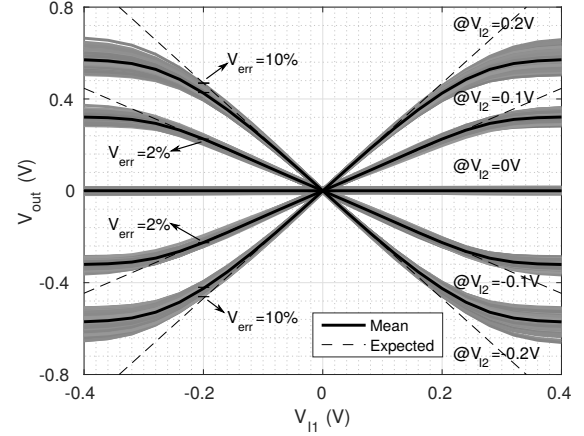


Fig. 6. DC transfer characteristics of the multiplier. Within the signal swing range of 200 mV the multiplier shows a maximum of 10% error at the output.

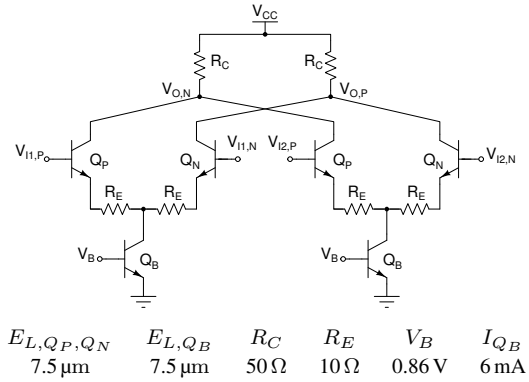
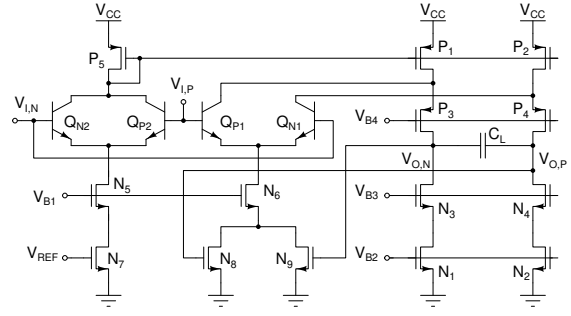


Fig. 7. Schematic of the adder. It has a DC gain of 12.3 dB and a bandwidth of 18.4 GHz.

maximum deviation from the linear region is only 10% in the signal swing of concern. A single multiplier occupies an area of  $\sim 40 \mu\text{m} \times 45 \mu\text{m}$ . A complex multiplier is implemented by connecting four such Gilbert cells, and a squaring circuit is implemented by giving the same signals to both inputs.

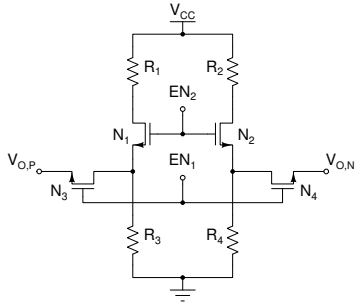
3) *Adder*: The addition operation is performed in the current domain by adding two current signals onto a common resistor. This technique is used in blocks such as complex multiplier where routing is minimal. When an additional gain is required, two CE sections are used with common load resistors, as shown in Fig. 7. The adder has a DC gain of 12.3 dB and a bandwidth of 18.4 GHz. For the convenient placement of adder circuit in the equalizer layout, the adder is designed as half circuits, each of which has an area of  $\sim 20 \mu\text{m} \times 40 \mu\text{m}$ .

4) *Integrator*: The settling behavior and steady-state error performance of the equalizer are primarily decided by the DC gain and cut-off frequency of the integrator, which makes it a critical building block. A folded BiCMOS amplifier topology with a large capacitive load is chosen to get a very high DC gain without compromising the pole locations. A circuit schematic of the integrator is shown in Fig. 8. The high gain amplifier of the integrator is a modified version of the basic folded cascode amplifier discussed in [32–34] and the  $G_m$  stage of the amplifier is designed with bipolar transistors as



$E_{L,QP1,2}$	$(W/L)_{N1,2}$	$(W/L)_{N3,4}$	$V_{B1}$	$V_{B2}$
0.6 $\mu\text{m}$	9.52/3	9.92/3	0.69 V	0.7 V
$E_{L,QN1,2}$	$(W/L)_{P1,2}$	$(W/L)_{P3,4}$	$V_{B3}$	$V_{B4}$
0.6 $\mu\text{m}$	141.84/3	72/3	1.4 V	1.1 V
$(W/L)_{N5,6}$	$(W/L)_{N7}$	$(W/L)_{N8,9}$	$V_{REF}$	$I_{N1}$
46/3	3.86/0.84	1.93/0.84	1.3 V	20 $\mu\text{A}$
	$(W/L)_{P5}$	$I_{N6}$	$C_L$	
	145.5/3	40 $\mu\text{A}$	7 pF	

Fig. 8. Schematic of a folded cascode BiCMOS integrator. The integrator has an area of  $\sim 120 \mu\text{m} \times 160 \mu\text{m}$  and a DC gain of 103.9 dB with a bandwidth of 56.2 Hz.



$(W/L)_{N1,2}$	20/0.28
$(W/L)_{N3,4}$	10/0.28
$R_1 + R_3$	1.4 k $\Omega$
$R_2 + R_4$	1.4 k $\Omega$

Fig. 9. Reset circuit for initializing weight coefficients of the equalizer. Voltage dividers consisting of  $R_1$  to  $R_4$  force the desired initial values of the weight coefficients.

suggested in [35]. To obtain a very low-frequency pole without affecting the high gain, the output resistance of the circuit has to be maximized. Hence, the cascode section of the amplifier is biased at a low current. The amplifier gain is given by [32]

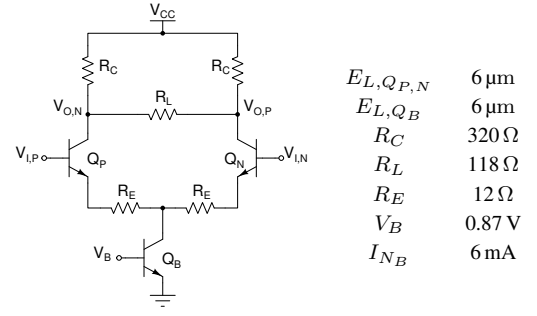
$$|A_V| \approx g_{m,QP1} \{ [(g_{m,P3} + g_{mb,P3})r_{o,P3}(r_{o,QP1} || r_{o,P1})] || [(g_{m,N3} + g_{mb,N3})r_{o,N1}r_{o,N3}] \}, \quad (8)$$

the output resistance is given by

$$R_O \approx [(g_{m,P3} + g_{mb,P3})r_{o,P3}(r_{o,QP1} || r_{o,P1})] || [(g_{m,N3} + g_{mb,N3})r_{o,N1}r_{o,N3}], \quad (9)$$

and the cut-off frequency is given by  $f_{3dB} \approx 1/2\pi R_O C_L$ . The integrator shown in Fig. 8 has a common-mode feedback (CMFB) structure that comprises transistors  $N_5$ - $N_9$  and the dummy transistors  $QP_2$  and  $QN_2$ . A detailed design of the CMFB can be found in [32]. The integrator has an area of  $\sim 120 \mu\text{m} \times 160 \mu\text{m}$  and a DC gain of 103.9 dB with a bandwidth of 56.2 Hz.

5) *Reset Circuit*: To initialize the weight coefficients, a reset circuit shown in Fig. 9 is used. An enable signal,  $EN_1$  is applied at the startup of the equalizer operation which turns on switches  $N_3$  and  $N_4$ . The enable signal  $EN_2$  is a delayed version of  $EN_1$  to avoid any unwanted discharge



$E_{L,QP,N}$	6 $\mu\text{m}$
$E_{L,QB}$	6 $\mu\text{m}$
$R_C$	320 $\Omega$
$R_L$	118 $\Omega$
$R_E$	12 $\Omega$
$V_B$	0.87 V
$I_{NB}$	6 mA

Fig. 10. Schematic of the output buffer. The buffer occupies an area of  $\sim 44 \mu\text{m} \times 46 \mu\text{m}$  and has a bandwidth of 37.8 GHz.

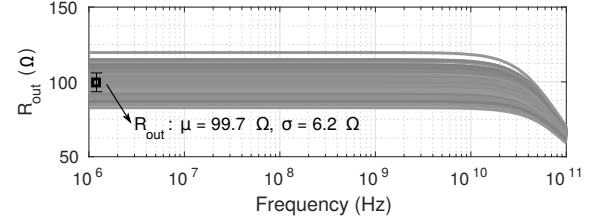


Fig. 11. Output resistance of the buffer. The differential output resistance is  $\sim 100 \Omega$  in the band of concern.

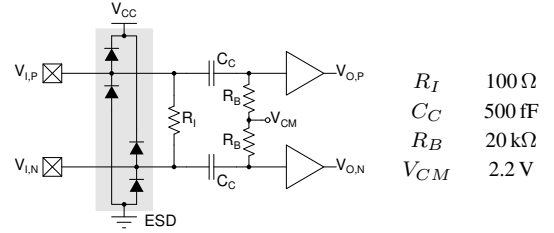


Fig. 12. Schematic of the circuit to match the input impedance. ESD: electrostatic discharge protection circuit.

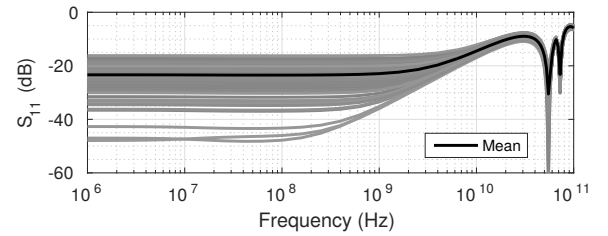


Fig. 13. Input reflection coefficient of the matching circuit.  $S_{11}$  is lower than  $-10 \text{ dB}$  in the band of concern.

of the integrator capacitor. Different combinations of  $R_1$  to  $R_4$  are chosen so as to initialize the weight coefficients at the integrator output nodes. When a global reset signal is asserted the equalizer tap coefficients are reset to the values  $\mathbf{h}_{xx} = [1 + j \ 0]^T$ ,  $\mathbf{h}_{xy} = [0 \ 0]^T$ ,  $\mathbf{h}_{yx} = [0 \ 0]^T$ , and  $\mathbf{h}_{yy} = [1 + j \ 0]^T$ .

6) *Output Buffer*: Outputs nodes of the equalizer are designed to drive high-speed transmission lines. To match impedance at the output nodes CE buffers are used, a schematic of as shown in Fig. 10. The parallel combination  $2R_C || R_L$  helps to match the impedance without decreasing the value of  $R_C$ . This configuration also helps to achieve different AC and DC output resistances while maintaining the

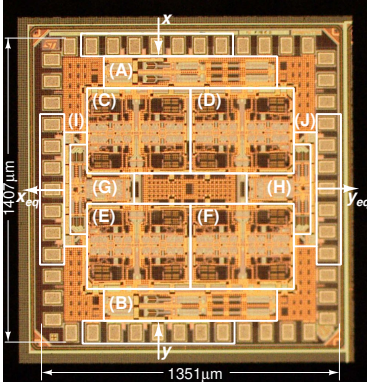


Fig. 14. Micro-graph of the equalizer IC. The block labels correspond to the explanation given in Fig. 2(b).

transistors in the active region of operation. The buffer has a DC gain of 4.9 dB and a bandwidth of 37.8 GHz. The output of the buffer, which occupies an area of  $\sim 44 \mu\text{m} \times 46 \mu\text{m}$  is matched, as shown in Fig. 11 with a differential output resistance of 99.7  $\Omega$ .

7) *Other Building Blocks*: Level shifters are used to shift common-modes up or down at various nodes, and AC coupling is used wherever this level shifting is not possible. All bias currents are mirrored from a single bias current which is supplied from outside. To match the impedance of high-speed inputs, the circuit shown in Fig. 12 is used. This configuration provides an input differential matching of 100  $\Omega$ , and the desired common mode to the input signals. There is also an electro-static discharge (ESD) protection circuit made up of ESD diodes. Simulations show an  $S_{11}$  parameter, which is better than -10 dB in the frequency band of concern, which is shown in Fig. 13.

### C. The Equalizer IC

A micrograph of the prototype equalizer is shown in Fig. 14, in which all the sub-blocks are marked corresponding to Fig. 2(b). The IC has 50 pads of which 28 are meant for high-speed differential signals which are arranged in a ground-signal-signal-ground-signal-ground (GSSGSSG) pattern. Rest of the pads are used for reset signal, bias current, amplitude control signals, and supply voltage and ground. The equalizer occupies  $\sim 1.4 \text{ mm} \times 1.35 \text{ mm}$  chip area and draws 1 A current from a 2.5 V supply.

## IV. RESULTS AND DISCUSSION

The equalizer is validated experimentally at 40 Gb/s data rate and by using post-layout simulations at 100 Gb/s data rate, details of which are given in the following sub-sections.

### A. Measurement Results at 40 Gb/s Data Rate

Fig. 15 shows a block diagram of the experimental setup with a 40 Gb/s DP-QPSK system. In the setup, an external cavity laser of 1550 nm wavelength is used as the carrier source at the transmitter. A 50:50 power splitter (PS) divides the laser output into two parts—one of which gets modulated

at the transmitter and the other is used as a local oscillator (LO) at the receiver. Two independent 10-Gb/s data streams are generated using a 10-Gb/s pseudo-random binary sequence generator which is clocked by a 10 GHz source. The two data streams are amplified (I and Q) to drive the nested Mach-Zehnder modulator (MZM) shown in the figure. The MZM gives out a 20-Gb/s QPSK modulated carrier which is split into X and Y polarizations using a polarization beam splitter (PBS). The X output of the PBS is directly connected to the X input of a polarization beam combiner (PBC), whereas the Y output is delayed using a 2 m-long polarization maintaining fiber before connecting to the Y input of the PBC. The optical delay is used to de-correlate the X and Y QPSK signals. The MZM-PBS-optical delay-PBC combination emulates a DP-QPSK modulator which gives out a 40 Gb/s DP-QPSK modulated carrier to the channel.

At the receiver side, the signal from the channel, S and the LO are fed to the inputs of an integrated coherent optical receiver front-end. The required power level of the LO is maintained using a variable optical attenuator (VOA), which is connected just before the receiver front-end. The receiver front-end consists of PBSs, optical hybrids, balanced photodiodes, trans-impedance amplifiers, and automatic gain control in the mentioned order. This module maintains a differential signal level of 400 mVpp on all four inputs ( $x_I$ ,  $x_Q$ ,  $y_I$ , and  $y_Q$ ) of the equalizer IC which is wire-bonded to a printed circuit board (PCB). The PCB shown in Fig. 16 is designed using RT duriod/6010LM laminate, more details of which can be found in [36]. The PCB has four pairs of input transmission lines and four pairs of output transmission lines which end on SMA connectors mounted along the periphery of the PCB. The outputs of the equalizer are stored using a 21 GHz real-time oscilloscope to process further using a behavioral model of a CPRC.

Fig. 17 depicts the block diagram of the behavioral CPRC that consists of a single sideband mixer, phase detector, loop filter, and quadrature-phase voltage controlled oscillator. Further details of the CPRC can be found in [30]. An error vector magnitude<sup>2</sup> (EVM) of the output signal is calculated by sampling the CPRC outputs at the maximum eye-opening point.

Performance of the equalizer is characterized using the 40 Gb/s system for different link lengths. Fig. 18 shows the eye-diagrams obtained at various stages of the experimental setup with a back-to-back optical link. The eye-diagram shown in Fig. 18(a) is that of the transmitted signal with 24% EVM. It may be noted that no pre-equalization or pre-compensation are performed to nullify the effects of components non-idealities, which resulted in a poor transmitter EVM. Fig. 18(b) shows the received signal eye-diagram, which is distorted due to the

<sup>2</sup>EVM of a signal in the I-Q space can be calculated as

$$EVM(\%) = \sqrt{\frac{\sum_{k=1}^N \{(I_k - \hat{I}_k)^2 + (Q_k - \hat{Q}_k)^2\}}{\sum_{k=1}^N (I_k^2 + Q_k^2)}} \times 100$$

where  $I_k$  is the I component of the  $k^{\text{th}}$  received symbol,  $Q_k$  is the Q component of the  $k^{\text{th}}$  received symbol,  $\hat{I}_k$  is the expected I component of the  $k^{\text{th}}$  received symbol,  $\hat{Q}_k$  is the expected Q component of the  $k^{\text{th}}$  received symbol, and  $N$  is the total number of received symbols.



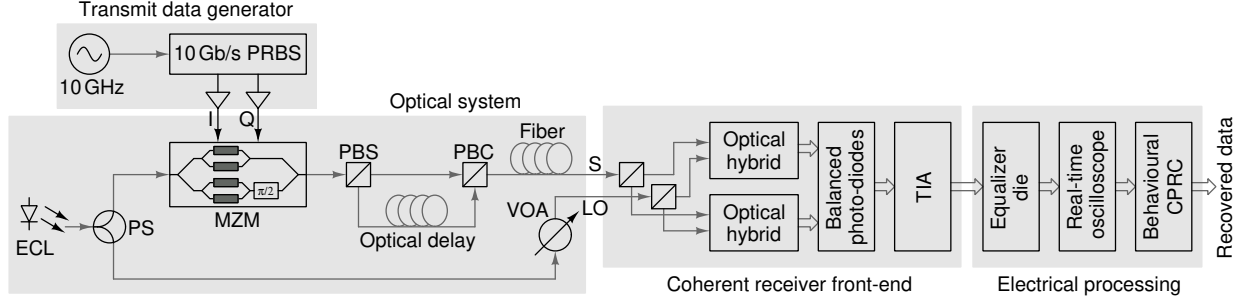


Fig. 15. Experimental setup with a 40 Gb/s DP-QPSK optical transmission system. PRBS: pseudo random binary sequence, I: in-phase data, Q: quadrature-phase data, ECL: external cavity laser, PS: power splitter, MZM: Mach-Zehnder modulator, PBS: polarization beam splitter, PBC: polarization beam combiner, VOA: variable optical attenuator, S: optical signal from the fiber channel, LO: local oscillator, TIA: trans-impedance amplifier, AGC: automatic gain control, and CPRC: carrier phase recovery and compensation.

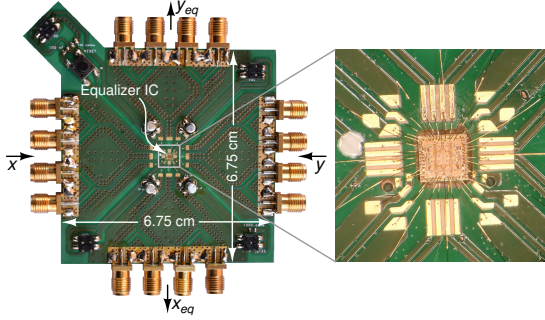


Fig. 16. PCB used to validate the CMA Equalizer. The equalizer IC is wire-bonded to the center of the PCB as shown in the inset.

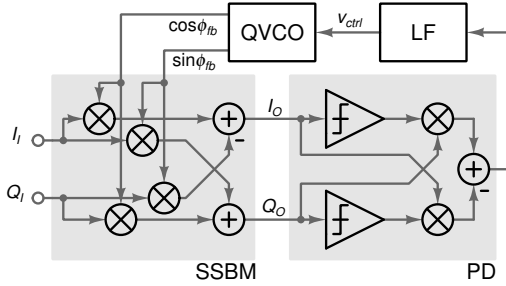


Fig. 17. Block-diagram of the decision-assisted Costas loop CPRC [30]. SSBM: single sideband mixer, PD: phase detector, LF: loop filter, and QVCO: quadrature-phase voltage controlled oscillator.

system non-idealities. Fig. 18(c) shows the equalizer output eye-diagram and Fig. 18(d) shows the CPRC output eye-diagram with 28% EVM which corresponds to an estimated bit error rate<sup>3</sup> (BER) of  $1.8 \times 10^{-4}$ .

X polarization constellations at various stages of the system are shown in Fig. 19 with results of a back-to-back link in the top row, a 5 km link in the middle row, and a 10 km link in the bottom row. Since the same laser is used at the transmitter and receiver, there is only a minimal phase offset between the received signal and LO at the receiver in the back-to-back

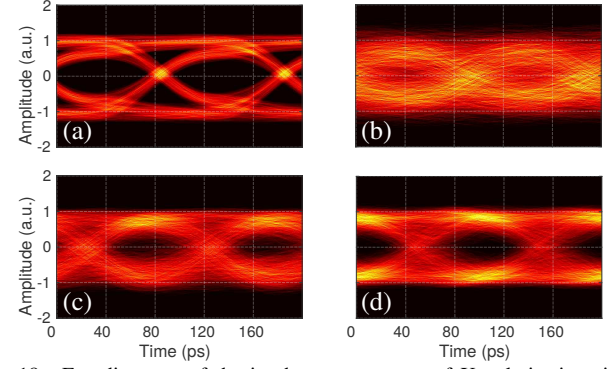


Fig. 18. Eye-diagrams of the in-phase component of X polarization signal at (a) transmitter, (b) equalizer input, (c) equalizer output, and (d) CPRC output in the experimental setup with a 40 Gb/s back-to-back link.

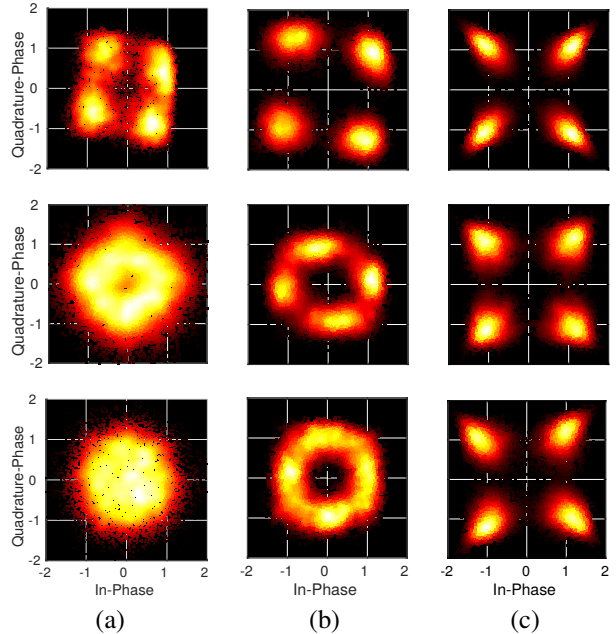


Fig. 19. X polarization constellations of the (a) received signal, (b) equalized signal, and (c) recovered signal in a 40 Gb/s back-to-back (top row), 5 km (middle row), and 10 km (bottom row) links.

<sup>3</sup>BER is estimated from the EVM as [37]

$$BER \approx \frac{2(1-1/P)}{\log_2 P} Q \left\{ \sqrt{\left( \frac{3 \log_2 P}{P^2 - 1} \right) \left( \frac{2}{EVM^2 \log_2 M} \right)} \right\}$$

where  $P$  is number of levels per dimension and  $M$  is the number of symbols on the I-Q plane.

link. Under such conditions, the equalizer can recover four constellation points, but with a slight rotation due to the phase insensitivity of the CMA algorithm. However, in 5 km and

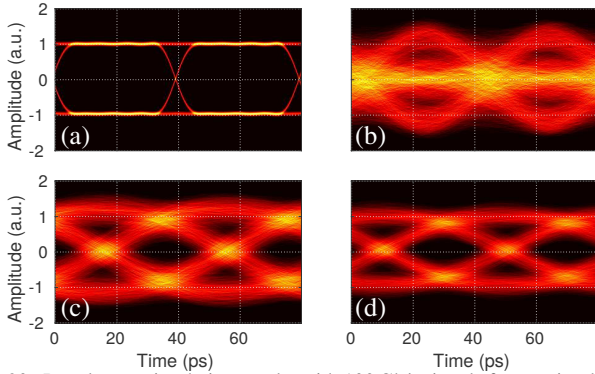


Fig. 20. Post-layout simulation results with 100 Gb/s signals from a simulation model of 5 km optical link. Eye-diagrams of the in-phase component of X polarization signals at the (a) transmitter, (b) equalizer input, (c) equalizer output, and (d) CPRC output.

10 km links, a large optical path difference between the signal and LO results in a frequency offset which is evident from the equalized constellation diagrams, which appear as rings on the I-Q plane. Post-processing carried out with the behavioral CPRC results in the constellations shown in Fig. 19(c) with an EVM of 28% in the back-to-back, 32% in the 5 km, and 33% in the 10 km links. The corresponding estimated pre forward error correction (pre-FEC) BERs are  $1.8 \times 10^{-4}$ ,  $8.9 \times 10^{-4}$ , and  $1.2 \times 10^{-3}$ , respectively, which are well below the hard-decision FEC limit. Similar constellations are obtained for the Y polarization also. Preliminary measurement results of the equalizer at a lower data rate were presented earlier in [28].

#### B. Post Layout Simulation Results at 100 Gb/s Data Rate

Due to the non-availability of a cost-effective packaging solution for high-speed ICs with a large pin count experimental validation of the equalizer at the designed data rate is not performed. Also, the small pad pitch of the IC limited the possibilities of an optimal direct die attach and a very well matched on-PCB transmission lines. Apart from these, issues owing to the bandwidth limitation due to bond-wire inductance, transmission lines, and SMA connectors functionality of the equalizer at 100 Gb/s is verified through post-layout simulations. A 100 Gb/s transmission system is modeled in VPItransmissionMaker from which the received signals are exported for circuit simulation after the O/E conversion. Fig. 20 shows the results of a post-layout simulation carried out in typical-typical corner with the data from a simulation model of an optical link with a 5 km SMF channel. Fig. 20(a) shows the eye-diagram of the transmitted data with an EVM of 1%, which becomes distorted when it reaches the receiver side, as shown in Fig. 20(b). Fig. 20(c) is the eye-diagram of the equalizer output and Fig. 20(d) is the output of a behavioral CPRC with an EVM of 27.8%. Performance analysis of the equalizer has been reported earlier in [30] using pre-layout circuit simulations.

Due to the issues of the cost-effective packaging mentioned earlier the measured performance of the equalizer is sub-optimal. A probe-card or a flip-chip-on-board assembly would have obtained a better performance from the IC, but such a setup would have been expensive since the pad-pitch is

very small. A fine-tuned optical system employing pulse shaping at the transmitter side to help with effective bandwidth utilization, a PCB with well-matched transmission lines, and a better thermal management system are also expected to improve the experimental setup. The major limiting factor of all-analog processing would be the bandwidth reduction due to the cascading effect. This would restrict the maximum amount of dispersion to be corrected since a larger amount of dispersion requires a larger number of cascaded taps in the equalizer. However, usage of on-chip transmission lines and a combination of active and passive delay lines would help to increase the number of taps to some extent. It is observed that the delay cells contribute significantly to the overall power consumption of the IC. However, by optimizing the delay cell design in the same node a significant reduction in the overall power consumption is also reported [38]. Usage of a lower node will help to reduce the power consumption, which may be inferred from [39, 40]. Implementation using FinFET technology is also expected to reduce power consumption and improve performance because of a higher transit frequency ( $f_T$ ) and a lower supply voltage. Other critical blocks at the receiver side are also being investigated successfully. For example, an analog domain Costas loop-based CPRC IC demonstration has been reported quite recently in [16]. These results give a clear indication that all-analog signal processing is a good solution for the power consumption-size-cost problem of the DCI transceivers.

#### V. CONCLUSION

The detailed architecture of a continuous-time adaptive equalizer that uses the CMA algorithm to update weight coefficients is presented. A two-tap prototype of the equalizer, which is meant for 100 Gb/s DP-QPSK coherent optical receivers, is implemented in a 130 nm BiCMOS technology and has an energy consumption of  $\sim 25$  pJ/bit. Experimental validation carried out with a 40 Gb/s back-to-back link shows an EVM which is very close to the transmitter EVM. Performance of the equalizer at 100 Gb/s data rate is verified through post-layout circuit simulations considering all the parasitics. The equalizer architecture can be extended for coherent optical communication systems that use higher order modulation formats to increase the data rate. Even though the results shown in this work correspond to 1550 nm wavelength the equalizer can be used with 1310 nm wavelength as well, thereby increasing the overall channel length. The promising results presented make the equalizer an ideal choice for short-reach optical links such as DCIs.

#### ACKNOWLEDGMENT

We would like to thank the Department of Science and Technology and Ministry of Electronics and Information Technology, Government of India for funding the project. We would also like to acknowledge Arvind Kumar Mishra and Madhan Thollabandi of Sterlite Technologies who gave us insight into optical system setup.



## REFERENCES

- [1] Cisco global cloud index: Forecast and methodology, 2016–2021 white paper. [Online]. Available: <https://www.cisco.com/c/en/us/solutions/collateral/service-provider/global-cloud-index-gci/white-paper-c11-738085.html>
- [2] Cisco visual networking index: Forecast and trends, 2017–2022 white paper. [Online]. Available: <https://www.cisco.com/c/en/us/solutions/collateral/service-provider/visual-networking-index-vni/white-paper-c11-741490.html>
- [3] The 2018 ethernet roadmap. [Online]. Available: <https://ethernetalliance.org/the-2018-ethernet-roadmap/>
- [4] M. Filer, S. Searcy, Y. Fu, R. Nagarajan, and S. Tibuleac, "Demonstration and Performance Analysis of 4 Tb/s DWDM Metro-DCI System with 100G PAM4 QSFP28 Modules," in *Proc. OFC*, Mar. 2017, p. W4D.4.
- [5] J.-P. Elbers *et al.*, "PAM4 vs Coherent for DCI Applications," in *Proc. SPPCom*. Optical Society of America, 2017, p. SpTh2D.1.
- [6] C. L. Schow, "Low Power Analog Coherent Links for Next-Generation Datacenters," in *Proc. CLEO*. Optical Society of America, 2019, p. STh4N.3.
- [7] M. Sharif, J. K. Perin, and J. M. Kahn, "Modulation Schemes for Single-Laser 100 Gb/s Links: Single-Carrier," *J. Lightw. Technol.*, vol. 33, no. 20, pp. 4268–4277, Oct. 2015.
- [8] K. Kikuchi, "Fundamentals of coherent optical fiber communications," *J. Lightw. Technol.*, vol. 34, no. 1, pp. 157–179, Jan. 2016.
- [9] E. Ibragimov, H. Jiang, P. Xu, and X. Li, "Coherent Analog Low Power, Small Size 400/200/100Gb/s Receiver Based on Bipolar SiGe Technology," in *Proc. OFC*, Mar. 2018, pp. 1–3.
- [10] P. Moyade, N. Nambath, A. Ansari, and S. Gupta, "Analog Processing Based Equalizer for 40 Gbps Coherent Optical Links in 90 nm CMOS," in *Proceedings of the International Conference on VLSI Design*, Jan. 2012, pp. 101–106.
- [11] J. K. Perin, A. Shastri, and J. M. Kahn, "Design of Low-Power DSP-Free Coherent Receivers for Data Center Links," *J. Lightw. Technol.*, vol. 35, no. 21, pp. 4650–4662, Nov. 2017.
- [12] M. Morsy-Osman *et al.*, "DSP-Free 'Coherent-Lite' Transceiver for Next Generation Single Wavelength Optical Intra-Datacenter Interconnects," *Opt. Express*, vol. 26, no. 7, pp. 8890–8903, Apr. 2018.
- [13] C. L. Schow and K. Schmidtke, "INTREPID: Developing Power Efficient Analog Coherent Interconnects to Transform Data Center Networks," in *Proc. OFC*. Optical Society of America, 2019, p. M4D.9.
- [14] M. Lu *et al.*, "An Integrated 40 Gbit/s Optical Costas Receiver," *J. Lightw. Technol.*, vol. 31, no. 13, pp. 2244–2253, July 2013.
- [15] J. Verbist *et al.*, "Real-Time 100 Gb/s NRZ and EDB Transmission with a GeSi Electroabsorption Modulator for Short-Reach Optical Interconnects," *J. Lightw. Technol.*, vol. 36, no. 1, pp. 90–96, Jan. 2018.
- [16] R. Ashok *et al.*, "Demonstration of an Analogue Domain Processing IC for Carrier Phase Recovery and Compensation in Coherent Links," in *Proc. OFC*, Mar. 2019, p. W2A.31.
- [17] B. S. G. Pillai *et al.*, "End-to-End Energy Modeling and Analysis of Long-Haul Coherent Transmission Systems," *J. Lightw. Technol.*, vol. 32, no. 18, pp. 3093–3111, Sep. 2014.
- [18] H. Wu, J. A. Tierno, P. Pepeljugoski, J. Schaub, S. Gowda, J. A. Kash, and A. Hajimiri, "Integrated Transversal Equalizers in High-Speed Fiber-Optic Systems," *IEEE J. Solid-State Circuits*, vol. 38, no. 12, pp. 2131–2137, Dec. 2003.
- [19] S. Pavan and R. Tiruvuru, "Analysis and Design of Singly Terminated Transmission-Line FIR Adaptive Equalizers," *IEEE Trans. on Circuits and Syst. I: Reg. Papers*, vol. 54, no. 2, pp. 401–410, Feb. 2007.
- [20] J. Hao, Z. Yumei, and J. Yishu, "A Low Power 3.125-Gbps CMOS Analog Equalizer for Serial Links," *J. Semiconductors*, vol. 31, no. 11, p. 115003, 2010.
- [21] W.-S. Kim and W.-Y. Choi, "A 10-Gb/s Low-Power Adaptive Continuous-Time Linear Equalizer Using Asynchronous Under-Sampling Histogram," *IEICE Electron. Express*, vol. 10, no. 4, pp. 1–8, 2013.
- [22] E. Mammei *et al.*, "Analysis and Design of a Power-Scalable Continuous-Time FIR Equalizer for 10 Gb/s to 25 Gb/s Multi-Mode Fiber EDC in 28 nm LP CMOS," *IEEE J. Solid-State Circuits*, vol. 49, no. 12, pp. 3130–3140, Dec. 2014.
- [23] Q. Pan *et al.*, "A 30-Gb/s 1.37-pJ/b CMOS Receiver for Optical Interconnects," *J. Lightw. Technol.*, vol. 33, no. 4, pp. 778–786, Feb. 2015.
- [24] A. Sharif-Bakhtiar and A. C. Carusone, "A 19.6-Gbps CMOS Optical Receiver with Local Feedback IIR DFE," in *Proc. VLSI Circuits*, Jun. 2015, pp. C116–C117.
- [25] P. C. Chiang *et al.*, "4×25 Gb/s Transceiver With Optical Front-end for 100 GbE System in 65 nm CMOS Technology," *IEEE J. Solid-State Circuits*, vol. 50, no. 2, pp. 573–585, Feb. 2015.
- [26] Q. Pan *et al.*, "A 30-Gb/s 1.37-pJ/b CMOS Receiver for Optical Interconnects," *J. Lightw. Technol.*, vol. 33, no. 4, pp. 778–786, Feb. 2015.
- [27] D. Lee, J. Han, G. Han, and S. M. Park, "An 8.5-Gb/s Fully Integrated CMOS Optoelectronic Receiver Using Slope-Detection Adaptive Equalizer," *IEEE J. Solid-State Circuits*, vol. 45, no. 12, pp. 2861–2873, Dec. 2010.
- [28] N. Nambath *et al.*, "First Demonstration of an All Analog Adaptive Equalizer for Coherent DP-QPSK Links," in *Proc. OFC*. Optical Society of America, Mar. 2017, p. M3D.5.
- [29] Y. Sato, "A method of Self-Recovering Equalization for Multilevel Amplitude-Modulation Systems," *IEEE Trans. Commun.*, vol. 23, no. 6, pp. 679–682, Jun. 1975.
- [30] N. Nambath *et al.*, "Analog Domain Signal Processing-Based Low-Power 100-Gb/s DP-QPSK Receiver," *J. Lightw. Technol.*, vol. 33, no. 15, pp. 3189–3197, Aug. 2015.
- [31] B. Gilbert, "A Precise Four-Quadrant Multiplier with Subnanosecond Response," *IEEE J. Solid-State Circuits*, vol. 3, no. 4, pp. 365–373, Dec. 1968.
- [32] B. Razavi, *Design of Analog CMOS Integrated Circuits*, ser. McGraw-Hill Higher Education. Tata McGraw-Hill, 2002.
- [33] P. Allen and D. Holberg, *CMOS Analog Circuit Design*. Oxford University Press, 2002.
- [34] P. R. Gray and R. G. Meyer, *Analysis and Design of Analog Integrated Circuits*, 5th ed. New York, NY, USA: John Wiley & Sons, Inc., 2009.
- [35] R. Krithivasan *et al.*, "A High-Slew Rate SiGe BiCMOS Operational Amplifier for Operation Down to Deep Cryogenic Temperatures," in *Proc. BCTM*, Oct. 2006.
- [36] N. B. Thaker, R. Ashok, S. Manikandan, N. Nambath, and S. Gupta, "Transmission Line Design for Testing High-Speed Integrated Circuits with Differential Signals," in *Proc. SPI*, Jun. 2019, pp. 1–4.
- [37] R. A. Shafik, M. S. Rahman, and A. R. Islam, "On the Extended Relationships Among EVM, BER and SNR as Performance Metrics," in *Proc. ICECE*, Dec. 2006, pp. 408–411.
- [38] S. R. Annadwar, N. Nambath, and S. Gupta, "Wideband Active Delay Cell Design for Analog Domain Coherent DP-QPSK Optical Receiver," in *Proc. VLSID*, Jan. 2016, pp. 213–218.
- [39] F. Loi, E. Mammei, S. Erba, M. Bassi, and A. Mazzanti, "A 25mW Highly Linear Continuous-Time FIR Equalizer for 25Gb/s Serial Links in 28-nm CMOS," *IEEE Trans. on Circuits and Syst. I: Reg. Papers*, vol. 64, no. 7, pp. 1903–1913, Jul. 2017.
- [40] K. Dasgupta *et al.*, "A 60-GHz Transceiver and Baseband With Polarization MIMO in 28-nm CMOS," *IEEE J. Solid-State Circuits*, vol. 53, no. 12, pp. 3613–3627, Dec. 2018.